Experimental Test of Curvature-Driven Dynamics in the Phase Ordering of a Two Dimensional Liquid Crystal

Alberto Sicilia,[1] Jeferson J. Arenzon,[2] Ingo Dierking,[3] Alan J. Bray,[3] Leticia F. Cugliandolo,[1] Josu Martínez-Perdiguero,[4] Ibon Alonso,[4] and Inmaculada C. Pintre[5]

[1]*Université Pierre et Marie Curie–Paris VI, LPTHE UMR 7589, 4 Place Jussieu, 75252 Paris Cedex 05, France*
[2]*Instituto de Física, Universidade Federal do Rio Grande do Sul, CP 15051, 91501-970 Porto Alegre RS, Brazil*
[3]*School of Physics and Astronomy, University of Manchester, Manchester M13 9PL, United Kingdom*
[4]*Departamento de Física de la Materia Condensada, Facultad de Ciencias, Universidad del País Vasco, Apartado 644, 48080 Bilbao, Spain*
[5]*Química Orgánica, Facultad de Ciencias, Instituto de Ciencia de Materiales de Aragón, Universidad de Zaragoza-CSIC, 50009 Zaragoza, Spain*
(Received 13 June 2008; published 7 November 2008)

We study electric field driven deracemization in an achiral liquid crystal through the formation and coarsening of chiral domains. It is proposed that deracemization in this system is a curvature-driven process. We test this prediction using the recently obtained exact result for the distribution of hull-enclosed areas in two-dimensional coarsening with nonconserved scalar order parameter dynamics [J. J. Arenzon *et al.*, Phys. Rev. Lett. **98**, 145701 (2007)]. The experimental data are in very good agreement with the theory. We thus demonstrate that deracemization in such bent-core liquid crystals belongs to the Allen-Cahn universality class, and that the exact formula, which gives us the statistics of domain sizes during coarsening, can also be used as a strict test for this dynamic universality class.

Many aspects of the nonequilibrium relaxation of macroscopic systems still remain to be grasped. The domain growth of two competing equilibrium phases after a quench from the disordered phase is a relatively simple out-of-equilibrium problem and in some cases the mechanism underlying coarsening is well understood (curvature driven, bulk diffusion, etc.) [1]. However, an important part of the description of these processes remains phenomenological and, to a certain extent, qualitative.

According to the scaling hypothesis, a system in the late stages of coarsening is described by a scaling phenomenology in which there is a single characteristic length scale, $R(t)$, that grows with time. As a consequence, all dynamical properties occurring on scales large compared to microscopic ones are described by scaling functions in which lengths are scaled by $R(t)$. For example, the pair-correlation function, $C(r, t) = \langle S(\mathbf{x}, t)S(\mathbf{x} + \mathbf{r}, t) \rangle$, where S takes the values ± 1 in the two equilibrium phases, has the scaling form $C(r, t) = g[r/R(t)]$ [1]. Verifying the scaling hypothesis, and computing the scaling functions, has been a long-standing challenge. Recently, however, significant progress was made when the distribution $n_h(A, t)$ of hull-enclosed areas (those enclosed by the outer boundaries of domains) was computed for scalar nonconserved order parameter dynamics in $d = 2$ and the scaling hypothesis verified for this quantity [2,3]. The analytically obtained distribution function was shown to be robust and hold—to a high numerical precision—in Monte Carlo simulations of the pure [2,3] and disordered [4] bidimensional kinetic Ising Model (2dIM). The question remains

as to whether more complicated experimental systems could also be described by such a universal formula.

In this Letter we test this result experimentally in a liquid crystal system and we find a very good agreement with the theory. We thus demonstrate that the system belongs to the universality class of nonconserved scalar order parameter dynamics and that the exact formula is a universal property of these systems. In the following paragraphs we describe the experiment and present a detailed analysis of the data.

The experimental system chosen is one that exhibits electric field driven deracemization, the spontaneous or driven formation of chiral domains from an achiral solution. Since its discovery by Louis Pasteur, more than 150 years ago [5], deracemization has been a fundamental question in the investigation of chirality. More recently, practical applications in, for example, drug design and synthesis, boosted research in this field, as the effect of most modern drugs is based on chiral molecules. Spontaneous deracemization in an achiral fluid system is very unusual and a topic of only recent interest [6]. It can occasionally be observed in liquid crystalline systems [7–9], mainly formed by bent-core or so-called "banana" molecules. The most likely reason for chiral conglomerate formation is steric interactions. This is also evidenced by computer simulations and theory, which indicate chiral conformations of on the average achiral molecules [10]. Electric field induced switching between chiral domains was demonstrated in Ref. [11]. Kane *et al.* [12] very recently exhibited the electric field driven deracemization

of an achiral fluid liquid crystalline system, and gave a theoretical interpretation of the conglomerate formation in terms of a difference in the chemical potential of left- and right-handed molecules under electric field application.

The liquid crystal employed in this investigation is composed of a bent-core molecule, which together with cell preparation conditions is discussed in detail in Ref. [13]. The studied cell has a gap of 5 μm filled with the liquid crystal, while lateral dimensions are much larger, approximately 1 cm in each direction. We are thus effectively investigating a two-dimensional system. Domain coarsening was followed by temperature controlled polarizing microscopy (Nikon Optiphot-Pol microscope in combination with a Linkham TMS91 hot stage), with a control of relative temperatures to 0.1 K. Digital images were captured at a time resolution of 1 s with a pixel resolution of $N = 1280 \times 960$, corresponding to a sample size of 520×390 μm^2 (JVC KY-F1030). Note that the imaging box is approximately 1/200 of the whole sample. Electric square-wave fields of amplitude $E = 14$ V μm^{-1} and frequency $f = 110$ Hz were applied by a TTi-TG1010 function generator in combination with an in-house built linear high voltage amplifier.

Cooling from the isotropic liquid, an optically isotropic fluid liquid crystal phase is formed, which exhibits no birefringence and thus appears dark between crossed polarizers. The phase transition is first order. On electric field application, chiral deracemization occurs with domains of opposite handedness growing as a function of time. This coarsening process can easily be followed when the polarizers are slightly decrossed by a few degrees. The chiral domains of opposite handedness get larger as smaller domains disappear. At the same time the area distribution of domains with opposite handedness remains constant at an equal distribution of left- and right-handed domains, because there is an overall constraint of zero chirality over the full sample that needs to be respected. This was checked experimentally and found to be true within experimental uncertainty due to finite size of the image window and thresholding. Still, such a global constraint (as opposed to a local one) is not expected to change the coarsening universality class which remains curvature driven [1].

We performed 10 runs lasting 10 min each with pictures taken at intervals of 10 s on a single sample. Each run is initialized by heating the sample above the transition temperature and subsequently cooling below it. The coarsening process in the low temperature phase is visualized in terms of domains, i.e., connected regions of the same handedness. In Fig. 1 we show a three snapshots taken at times $t = 0, 120, 300$ s. These pictures are then thresholded and an Ising spin s_i is assigned to each pixel, where $s_i(t) = \pm 1$ for pixels that belong to left- or right-handed domains, respectively. There are many spurious small domains that are related to the experimental system [14] rather than to thermal fluctuations. The induced graininess is also reflected in the small r behavior of the pair-
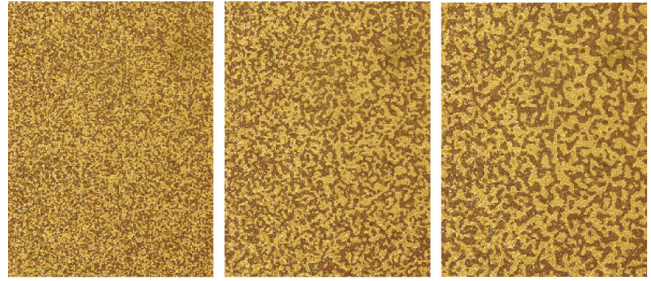

FIG. 1 (color online).   The first snapshot displays the configuration right after the quench, $t = 0$ s. The others are snapshots during the evolution $t = 120, 300$ s.

correlation function $C(r, t)$ and the small A behavior of $n_h(A, t)$ as we shall see below. Still, at face value the domain geometry is the one of scalar nonconserved order parameter dynamics, as can be checked by comparing to the snapshots shown in [3] for the 2dIM.

The initial "magnetization density" in the imaging window of the liquid crystal, defined as the average of the spin variables over the box, $m(0) = N^{-1} \sum_{i=1}^{N} s_i(0)$, is not zero. This initial value is only approximately conserved by the dynamics, $m(t) \approx m(0) = 0.2 \pm 0.1$, but the actual value depends on the thresholding operation.

We determine the growth law for the size, $R(t)$, of typical domains from a direct measure of the spatial correlation function, $C(r, t) \equiv \frac{1}{N} \sum_{i=1}^{N} \langle s_i(t)s_j(t) \rangle |_{|\vec{r}_i - \vec{r}_j|=r}$. The angular brackets indicate an average over the 10 runs. Here and in what follows, we measure distances in units of the pixel size ($a \simeq 2.5$ μm) and time in seconds for the experiments, while for the simulations we will use the lattice spacing and the Monte Carlo step as length and time units. The distance dependence of the pair correlation at five equally spaced times, $t = 100, \ldots, 500$ s is displayed with thin (red) lines in Fig. 2(a). As a consequence of the nonzero magnetization, $C(r, t)$ does not decay to zero at large r. More strikingly, the curves are time independent at distances $r \lesssim 5$ ($C \gtrsim 0.55$) and they clearly depend on time at longer distances with a slower decay at longer times. The time independence at short distances and the long-distance decay are atypical, as can be seen by comparing to the spatial correlation in the 2dIM displayed in the inset to Fig. 2(a). We ascribe the lack of time dependence at short scales and the further slow decay to the graininess of the experimental system. Indeed, in Fig. 2(a) we also show with thick dashed (black) lines the correlation in the 2dIM where we have flipped, at each measuring instant, 10% of spins taken at random over the sample (the system dynamics are not perturbed and between measurements we use the original spins). By comparing the two sets of curves we see that the effect of the random spins is similar to the one introduced by the graininess of the system. This effect will also be important for the analysis of the hull-enclosed area distribution.

The function $C(r, t)$ obeys dynamical scaling, $C(r, t) \simeq g[r/R(t)]$. We define the characteristic length scale $R(t)$ at

time t by the condition $C(R, t) = 0.2$ but other choices give equivalent results. The good quality of the scaling is shown in Fig. 2(b). The time dependence of the growing length $R(t)$ is shown in the inset to Fig. 2(b) with points. The error bars are estimated from the variance of the values obtained from the 10 independent runs. We measure the growth exponent $1/z$ by fitting the long-time behavior of $R(t)$, say for $t > 30$ s, and we find $1/z \simeq 0.45 \pm 0.10$. The exponent thus obtained is close to the theoretically expected value $1/2$ for clean nonconserved order parameter dynamics [1]. The data suggest that for times longer than $t \simeq 30$ s the system is well in the scaling regime.

We now turn to the analysis of the distribution of hull-enclosed areas. Each domain has one external perimeter which is called the *hull*. The *hull-enclosed area* is the total area contained within this perimeter. In [2,3] we derived an exact analytical expression for the hull-enclosed area distribution of curvature-driven two-dimensional coarsening with nonconserved order parameter. Using a continuum description in which the nonconserved order parameter is a scalar field we found that the number of hull-enclosed areas per unit area, $n_h(A, t)dA$, with enclosed area in the

interval $[A, A + dA]$, after a quench from high temperatures is

$$n_h(A, t) = 2c_h/(A + \lambda_h t)^2. \tag{1}$$

$c_h = 1/8\pi\sqrt{3}$ is a universal constant that enters this expression through the influence of the initial condition and was computed by Cardy and Ziff in their study of the geometry of critical structures in equilibrium [15]. λ_h is a material dependent constant relating the local velocity v of an interface and its local curvature κ, in the Allen-Cahn equation, $v = -(\lambda_h/2\pi)\kappa$ [16]. Equation (1) can be recast in the scaling form $n_h(A, t) = (\lambda_h t)^{-2} f(A/\lambda_h t)$, with $f(x) = 2c_h/(x + 1)^2$. In this way, scaling with the characteristic length scale, $R(t) = \sqrt{\lambda_h t}$, for coarsening dynamics with scalar nonconserved order parameter in a pure system is demonstrated.

We counted the number of hull-enclosed areas in $[A, A + dA]$ to construct $n_h(A, t)$. It is important to note that although the zero-chirality constraint should be satisfied by the full sample, the experimental data are taken using a
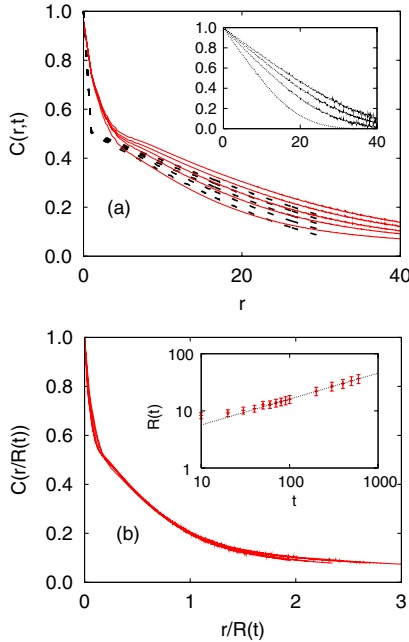

FIG. 2 (color online). Spatial correlation function at different times after the quench. (a) Experimental data at five equally spaced times, $t = 100, \ldots, 500$ s with thin (red) lines, and numerical simulation data in the 2dIM with 10% randomly flipped spins at five equally spaced times, $t = 100, \ldots, 500$ MCs with dashed (black) lines. We clearly notice the effect of graininess at very small scales ($r \lesssim 5$ in the experiment and $r \lesssim 1$ in the simulation), where there is no time dependence in either case. Inset: the actual spatial correlation in the 2dIM. (b) Study of the scaling hypothesis, $C(r, t) \simeq g[r/R(t)]$ in the liquid crystal, at the same times as in panel (a). Inset: the time dependence of the growing-length scale. The slope of this line is $1/z \simeq 0.45 \pm 0.10$.
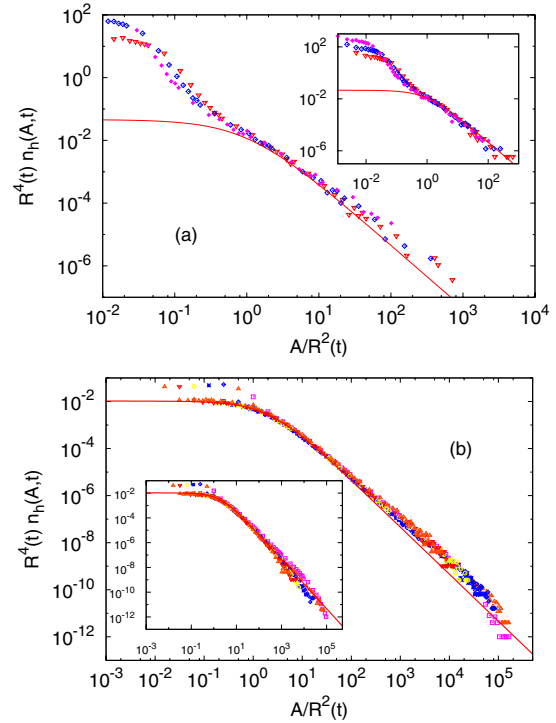

FIG. 3 (color online). Scaling plot of the number density of hull-enclosed areas in: (a) the experiment; (b) the 2dIM with linear size $L = 1280$ and periodic boundary conditions evolving with nonconserved order parameter at $T = 0$. In the latter the measurements are done on a box with linear size $\ell = 1000$. The lines are the prediction in Eq. (1). In the 2dIM case we exclude the spanning clusters from the statistics. In the insets we exclude all domains that touch the border while in the main panels we include them in the statistics. Surprisingly, in both cases $\lambda_h = 2.1$, although this is just a coincidence since λ_h is not a universal quantity and length and time units are different between experiments and simulations.
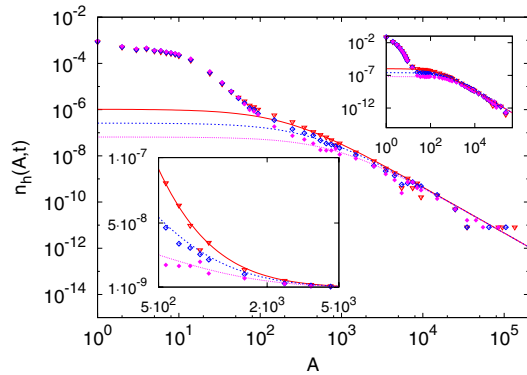
FIG. 4 (color online). The number density of hull-enclosed areas for the liquid crystal sample at $t = 100, 200, 400$ s, excluding from the analysis the areas that touch the box border. Lower inset: zoom-in of the interesting region using a log-lin scale. Upper inset: n_h for the 2dIM with 10% randomly flipped spins at the measurement times $t = 100, 200, 400$ MCs (see the text). In both cases the lines are the theoretical prediction (1) with $c_h = 1/8\pi\sqrt{3}$ and $\lambda_h = 2.1$.

finite imaging window inside the sample: at each measuring time, many domains touch the window boundaries (in contrast to the numerical simulations in [2–4] in which we used periodic boundary conditions). The zero-chirality constraint is thus not obeyed exactly, both because the image window is just a subset of the whole sample and also because of the thresholding operation.

In Fig. 3(a) we show the hull-enclosed area distribution in the liquid crystal at three different times. In the main panel we included in the statistics the chopped areas that touch the border of the image. The upward deviation of the data with respect to the asymptotic power law A^{-2} is due to the finite image size. Indeed, domains that touch the border are actually larger but get chopped and contribute to bins of smaller A's and this induces a bias in the data. The inset displays n_h removing from the statistics the areas that touch the border. The same anomaly appears in the 2dIM if one uses a finite imaging box within the bulk. To show this we simulated a system with $L = 1280$ and periodic boundary conditions and we measured n_h in a finite square window with linear size $\ell = 1000$ using 100 independent samples. In Fig. 3(b) we show two sets of data for the 2dIM; in both cases we exclude the spanning cluster over the full system size. One set of data includes areas touching the border and lies above the theoretical curve. In the other set we eliminated these areas from the statistics and the data points fall on the analytic curve recovering the A^{-2} tail.

The data in Fig. 4 do not show any noticeable time dependence at either small or large areas. In the small A limit the time independence can be traced back to the lack of time dependence in $C(r, t)$ at distances $r \lesssim 5$ (which corresponds to $A \simeq \pi r^2 \lesssim 80$), roughly the scale of the spatial graininess (see Fig. 2). In the large A limit the time dependence naturally disappears; structures with $A \gg$

$R^2(t)$ are basically the ones already present in the initial condition and have not had time to evolve yet. In between these two limits the curves show a shoulder with a systematic time dependence that is the most relevant part of our experimental data and it is very well described by the analytic prediction (1) shown with solid lines. To conclude we show that the random spins introduced by the measuring method are not only responsible for the time independence of n_h at small A but also for the excess weight of the distribution in this region. In the upper inset to Fig. 4 we show n_h in the 2dIM where we introduced 10% random spins at each measuring time. There is indeed a strong similarity with the experimental data in the main panel that could even be improved by choosing to flip spins in a fine-tuned correlated manner. In the lower inset we show a zoom-in of the interesting region using a log-lin scale.

In summary, our experimental results for the hull-enclosed area distribution in the coarsening dynamics of the liquid crystal are in very good agreement with the exact analytic prediction for 2D nonconserved scalar order parameter dynamics presented in [2,3]. The experiment was performed using an optimal choice of parameters (electric field, thresholding procedure, temperature, frequency, sample geometry, etc.). Although we do not expect our qualitative results to change it would be interesting to perform a detailed analysis of their effect on quantitative features such as the value of λ_h.

[1] A. J. Bray, Adv. Phys. **43**, 357 (1994).
[2] J. J. Arenzon *et al.*, Phys. Rev. Lett. **98**, 145701 (2007).
[3] A. Sicilia *et al.*, Phys. Rev. E **76**, 061116 (2007).
[4] A. Sicilia *et al.*, Europhys. Lett. **82**, 10 001 (2008).
[5] L. Pasteur, C. R. Hebd. Seances Acad. Sci. **26**, 535 (1848).
[6] Y. Takanishi *et al.*, Angew. Chem., Int. Ed. **38**, 2353 (1999).
[7] J. Thisayukta *et al.*, J. Am. Chem. Soc. **122**, 7441 (2000).
[8] G. Heppke *et al.*, Liq. Cryst. **27**, 313 (2000).
[9] N. V. S. Rao *et al.*, J. Mater. Chem. **13**, 2880 (2003).
[10] D. J. Earl *et al.*, Phys. Rev. E **71**, 021706 (2005).
[11] A. Eremin *et al.*, Phys. Rev. E **67**, 020702(R) (2003).
[12] A. Kane *et al.*, Chem. Phys. Chem. **8**, 170 (2007).
[13] J. Martinez-Perdiguero *et al.*, Phys. Rev. E **77**, 020701(R) (2008).
[14] The graininess appears to be related to electrohydrodynamic cells formed during electric field application. Their effects have been minimized as far as possible by the choice of electric field. The order of magnitude length scale is that of the cell gap, 5 μm, which would be consistent with electrohydrodynamic pattern formation.
[15] J. Cardy and R. M. Ziff, J. Stat. Phys. **110**, 1 (2003).
[16] S. M. Allen and J. W. Cahn, Acta Metall. **27**, 1085 (1979).